Conformational and Thermal Phase Behavior of Oligomethylene Chains Constrained by Carbohydrate Hydrogen-Bond Networks

Mitsutoshi Masuda,*,† Volkmar Vill,‡ and Toshimi Shimizu†

Contribution from the Department of Organic Materials, National Institute of Materials and Chemical Research, 1-1 Higashi, Tsukuba, Ibaraki 305-8565, Japan, and Institut für Organische Chemie, Universität Hamburg, Martin-Luther-King Platz 6, D-20146 Hamburg, Germany

Received May 30, 2000

Abstract: The oligomethylene spacer conformation and phase transition behavior of a series of *N*,*N*′-bis(β-D-glucopyranosyl)alkane-1,*n*-dicarboxamides [**1(*n*)**, $n = 6-14$, 16, 18, and 20] in a self-assembled solid state has been investigated using DSC, XRD, light microscopy, and FT-IR measurements. Both the chain conformation and thermal behavior of the assemblies have been used to classify them into three categories, short ($6 \le n \le 8$, and $n = 10$), medium ($n = 9$, and $11 \le n \le 13$), and long chain ($14 \le n \le 20$). Thus, the bolaamphiphiles with a short-chain spacer self-assembled in water to form a *gauche*-including monolayered self-assembly, while the medium- and long-chain homologues formed monolayered assemblies with an all-*trans* oligomethylene conformation. The short- and long-chain bolaamphiphiles also exhibited a polymorphism on heating which proceeded with retention of the *gauche* chain conformation, with the long-chain homologues transforming from the K1 crystalline phase to the K2 crystalline phase (keeping an all-*trans* conformation) and eventually into the K3 crystalline phase with a *gauche*-including spacer. In addition, the long-chain, **1(*n*)**, and medium-chain, **1(13)**, bolaamphiphiles formed a thermotropic mesophase (smectic A).

Introduction

Oligomethylene chains have been widely used as components of biomembrane lipids, glycelides, and synthetic amphiphiles[1−5] with substituents in the chain, the overall molecular shape and conditions during the assembly process all able to significantly affect the chain conformation and stability of the assemblies formed. The introduction of a weak binding interaction (for example, via hydrogen bond donors and acceptors) into the amphiphile headgroup can dramatically stabilize a self-assembled bilayer membrane (BLM) structure by constraining the conformation of the oligomethylene chain.[6] Bolaamphiphiles, in which two hydrophilic groups are connected to both ends of a hydrophobic spacer are even able to form stable monolayer membranes (MLMs). Indeed *Archaebacteria*, which survives even under such harsh conditions as pH 2 and 80 °C,[7,8] includes such hydrogen-bonded dumbbell-shaped sugar lipids as a key membrane component.

The constraining hydrogen bond networks also enforce a conformational deviation from the extended form upon the oligomethylene chain. We have previously found an unusual *kink* (*gauche*−*trans*−*gauche*′) or a *trans*−*gauche*−*staggered* conformation for the oligomethylene spacers in crystals of sugar-[9,10] and peptide-based bolaamphiphiles,[11] respectively. Similar conformational defects can be seen for other bolaamphiphilic molecules not only in the crystal lattice[12,13] but also in monolayer films adsorbed on a substrate.[14] A typical example was manifested by ω-terminated alkanethiol SAMs on metal surfaces[15−18] where an ω-terminal group (e.g., a carboxylic acid or an amide) forms a hydrogen-bonded network while the S atom binds to the metal surface, thereby constraining the oligomethylene chain at both ends. Hydrogen bonds between the bulky headgroups of sugar-based bolaamphiphillic MLMs impose similar conformational constraints on the oligomethylene chain. In this report we describe and classify the thermal phase transition and conformational behavior of the oligomethylene spacers in **1(*n*)** from the viewpoint of chain-length and headgroup effect (Scheme 1).

Scheme 1

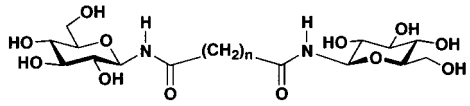

1(n): n = 6–14, 16, 18, and 20

* To whom correspondence should be addressed.
† National Institute of Materials and Chemical Research.
‡ Universität Hamburg.

(1) Okahata, Y.; Kunitake, T. *J. Am. Chem. Soc.* **1979**, *101*, 5231−5234.
(2) Fuhrhop, J.-H.; Köning, J. *Membranes and Molecular Assemblies: The Synkinetic Approach*, 1st ed.; The Royal Society of Chemistry: Cambridge, UK, 1994.
(3) Shimizu, T. *Trans. Mater. Res. Soc. Jpn.* **1999**, *24*, 431−436.
(4) Nuzzo, R. G.; Allara, D. L. *J. Am. Chem. Soc.* **1983**, *105*, 4481−4483.
(5) Bain, C. D.; Troughton, E. B.; Tao, Y.-T.; Evall, J.; Whitesides, G. M.; Nuzzo, R. G. *J. Am. Chem. Soc.* **1989**, *111*, 321−335.
(6) Fuhrhop, J.-H.; Helfrich, W. *Chem. Rev.* **1993**, *93*, 1565−1582.
(7) Gulik, A.; Luzzati, V.; de Rosa, M.; Gambacorta, A. *J. Mol. Biol.* **1985**, *182*, 131−149.
(8) Gliozzi, R. M.; Rolandi, R.; de Rosa, M.; Gambacorta, A. *J. Membr. Biol.* **1983**, *75*, 45−59.
(9) Shimizu, T.; Shibakami, M.; Masuda, M. *Chem. Lett.* **1997**, 267−268.
(10) Masuda, M.; Shimizu, T. *Carbohydr. Res.* **2000**, *326*, 56−66.
(11) Kogiso, M.; Masuda, M.; Shimizu, T. *Supramol. Chem.* **1998**, *9*, 183−189.
(12) Fahrnow, A. M.; Saenger, W.; Fritsch, D.; Schnieder, P.; Fuhrhop, J.-H. *Carbohydr. Res.* **1993**, *242*, 11−20.
(13) Zuniga, F. J.; Chapuis, G. *Mol. Cryst. Liq. Cryst.* **1985**, *128*, 349−366.
(14) Allara, D. L.; Atre, S. V.; Elliger, C. A.; Snyder, R. G. *J. Am. Chem. Soc.* **1991**, *113*, 1852−1854.
(15) Sun, L.; Crooks, R. M. *Langmuir* **1993**, *9*, 1775−1780.

10.1021/ja001884p CCC: $19.00
Published on Web 11/18/2000

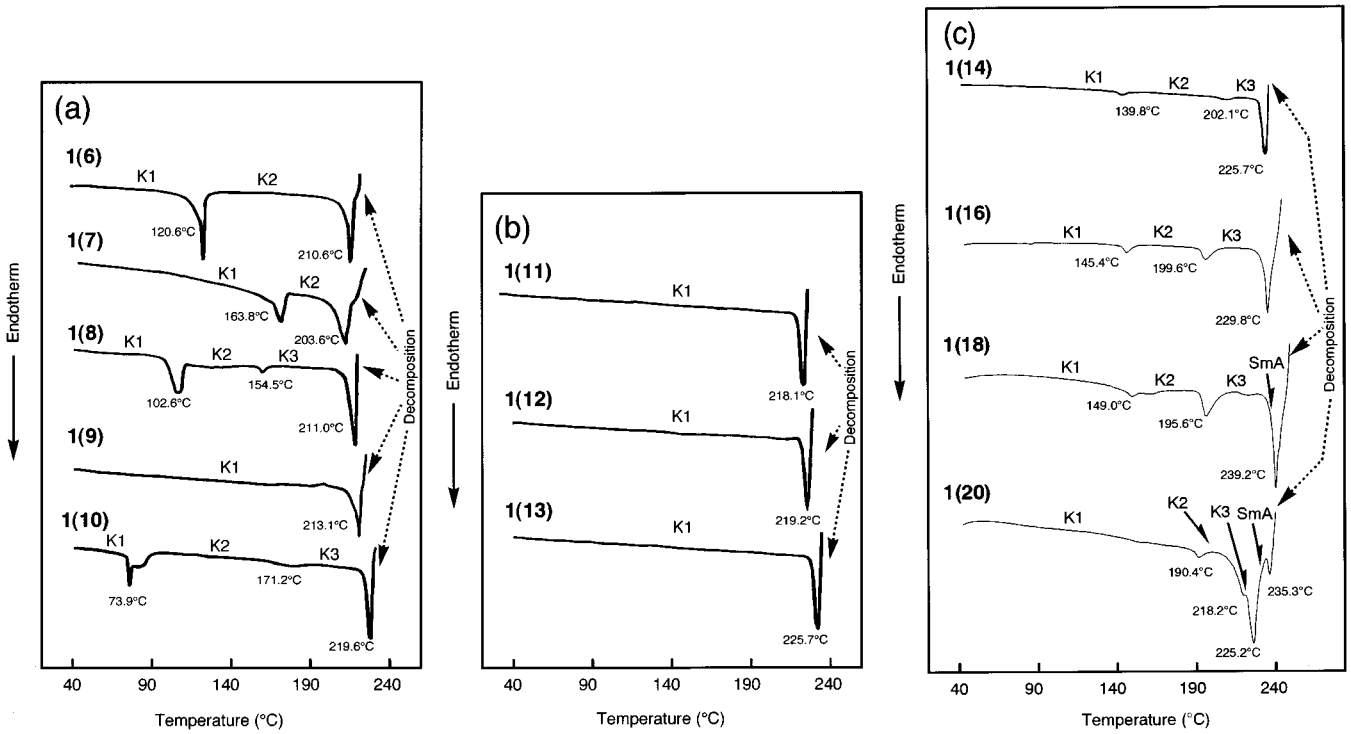

Figure 1. DSC traces of bolaamphiphiles, **1(*n*)**, (a) ($n = 6-10$), (b) ($n = 11-13$), and (c) ($n = 14$, 16, 18, and 20) on the first heating cycle.

Results

Unless otherwise noted, all of the self-assembled samples of **1(*n*)** were prepared by slow cooling and evaporation of the saturated aqueous solutions as reported elsewhere.[19] A ground single crystal of the bolaamphiphile **1(11)**[20] was also analyzed.

Thermal Phase Behavior by DSC. To examine the phase transition behavior of the oligomethylene spacers, we measured DSC profiles for the self-assemblies derived from **1(*n*)**. On the basis of these experiments, the oligomethylene chains of **1(*n*)** could be categorized into polymorphic short ($6 \le n \le 8$, and $n = 10$), nonpolymorphic medium ($n = 9$, and $11 \le n \le 13$), and polymorphic long chains ($14 \le n \le 20$) (Figure 1a−c). DSC traces of **1(*n*)** on the first heating cycle indicated that both short-chain **1(*n*)** ($n = 6-8$, and 10) and long-chain **1(*n*)** ($n =$ 14, 16, 18, and 20) homologues exhibit crystal polymorphism before isotropic melting (K1−K2 and K1−K2−K3 phase transitions, Figure 1a−c), contrasting with the medium-chain derivatives ($n = 9$, 11, 12, and 13) which showed no such polymorphism (Figure 1a and b). The anomalous behavior of **1(9)** and **1(10)** at the boundary of the short/medium groups arises from an even−odd effect of the chain length which will be discussed more fully hereafter. In addition, the existence of a mesophase was discovered for the bolaamphiphiles **1(18)** and **1(20)**. In all the experiments, cooling from the isotropic melt produced no reproducible peaks since **1(*n*)** is liable to decompose thermally upon melting.

The K2−K3 phase transition of the short-chain bolaamphiphiles **1(8)** and **1(10)** was reversible over multiple heating and cooling cycles, as were all K1−K2−K3 phase transitions of the long-chain homologues ($n = 14$, 16, 18, and 20). The reversibility can be only achieved when the heating cycles were stopped before melting and decomposing. The ΔH values for the reversible peaks were very small, showing that the crystalline polymorphism stems from packing or conformational changes of the oligomethylene chains, or partial dissociation of the hydrogen bond network.

Table 1. VT-XRD Data of Self-Assembled Bolaamphiphiles **1(*n*)**

chain length (n)	phase	XRD patterns (nm): long spacing (d)	XRD patterns (nm): short spacing
6	K1	2.18	0.447, 0.418, 0.370
	K2	2.00	0.448, 0.430, 0.381
7	K1	2.24	0.44[b]
	K2	2.15	0.44[b]
8	K1	2.26	0.44[b]
	K2	2.14	0.447, 0.418, 0.380
	K3	2.16	0.444, 0.425, 0.386
10	K1	2.46	0.44[b]
	K2	2.31	0.426, 0.401, 0.377
	K3	2.31	0.443, 0.415, 0.39−0.38
14	K1	2.61	0.425, 0.403, 0.380
	K2	2.60	0.444, 0.415, 0.39−0.38
	K3	2.67	0.468, 0.445, 0.388
16	K1	2.76	0.438, 0.391, 0.371
	K2	2.80	0.451, 0.428, 0.383
	K3	2.87	0.456, 0.39−0.38
18	K1	2.92	0.447, 0.404, 0.385
	K2	2.94	0.441, 0.416, 0.384
	K3	3.06	0.466, 0.445, 0.388
	SmA	2.95[c]	0.44[b,c]
20	K1	3.17	0.445, 0.413, 0.398
	K2	3.31	0.45[b]
	K3	n.d.[a]	0.45[b]
	SmA	3.04	0.48[b]

[a] Not determined. [b] Broad peak. [c] Measured at room temperature for the super cooled smectic A sample.

Variable Temperature XRD (VT-XRD). Table 1 summarizes the results of VT-XRD measurement for each phase of **1(*n*)** ($n = 6$, 7, 8, 10, 14, 16, 18, and 20) discovered in the DSC measurements. In general, the oligomethylene chains in

(16) Nuzzo, R. G.; Dubois, L. H.; Allara, D. L. *J. Am. Chem. Soc.* **1990**, *112*, 558−569.
(17) Troughton, E. B.; Bain, C. D.; Whitesides, G. M. *J. Am. Chem. Soc.* **1988**, *4*, 365−385.
(18) Laibinis, P. E.; Whitesides, G. M. *J. Am. Chem. Soc.* **1992**, *114*, 1990−1995.
(19) Shimizu, T.; Masuda, M. *J. Am. Chem. Soc.* **1997**, *119*, 2812−2818.

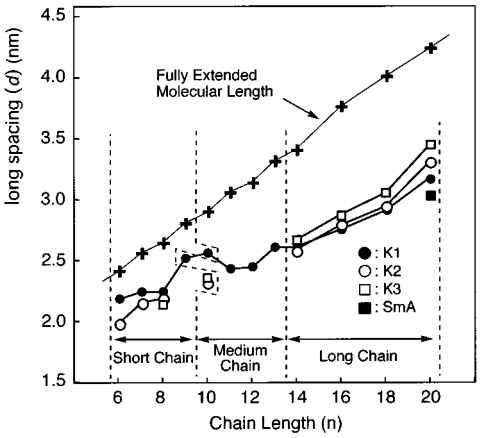

Figure 2. Dependence of fully extended molecular lengths and the long spacings (*d*) obtained from XRD patterns on the oligomethylene spacer length (*n*) of the self-assembled **1(*n*)** in each phase.

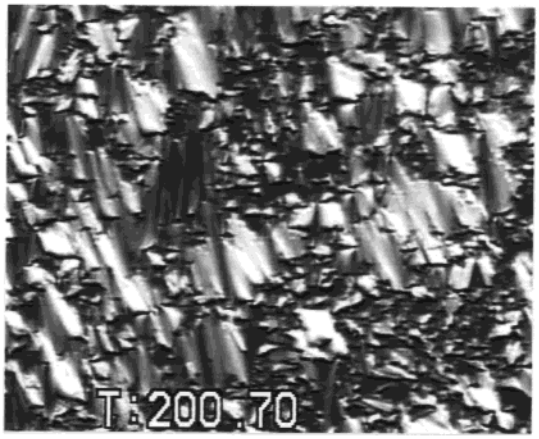

Figure 3. Polarized light micrograph of the mesophase observed for **1(20)** at 200.7 °C on cooling from the isotropic phase.

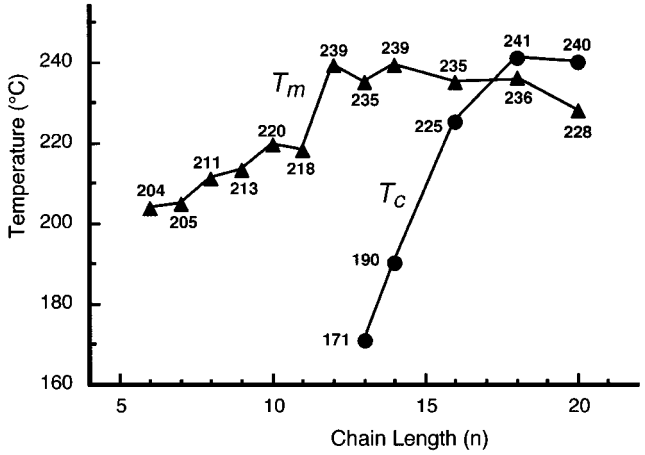

Figure 4. Melting- and clearing temperature of **1(*n*)** as a function of the oligomethylene spacer length (*n*).

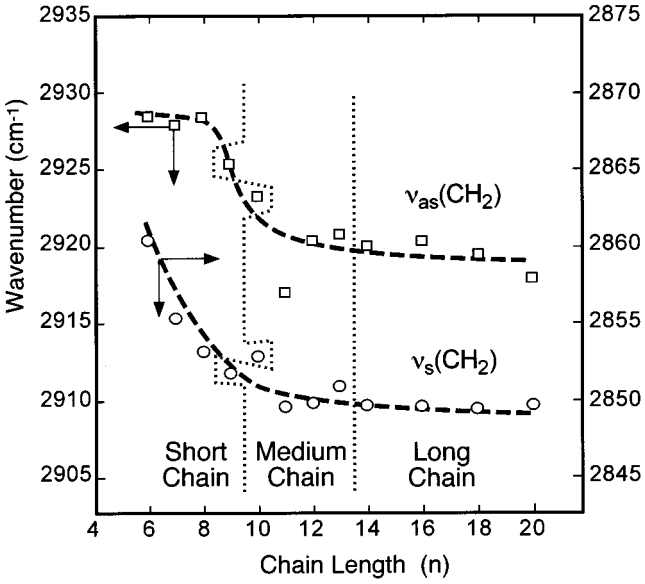

Figure 5. The dependence of the $\nu_{as}(CH_2)$ and $\nu_s(CH_2)$ band frequencies on the oligomethylene spacer length (*n*) for self-assembled **1(*n*)**.

the solid state are highly crystalline since the XRD patterns of most of **1(*n*)** showed several sharp reflection peaks around $d = 0.38-0.45$ compatible with a layered structure, which is similar to those of the bolaamphiphiles **1(*n*)** ($n = 11-14$) reported previously.[19,20] The long spacing (*d*) of **1(*n*)** estimated from small angle XRD was plotted against the oligomethylene chain length **(*n*)**, compared with calculated lengths from extended chain CPK molecular models (Figure 2). This again reveals the existence of three categories. The long spacing (*d*) of the short-chain homologues **1(*n*)** ($n \leq 10$) shrinks on heating, while that of the long-chain homologues ($n \geq 14$) widens. While the liquid crystalline phase of **1(18)** proved unstable for XRD measurement and thus could not be accurately investigated, the *d* spacing of the **1(20)** mesophase is smaller than those of the crystalline K1, K2, and K3 phases in good agreement with smectic phases formed by other bolaamphiphiles.[21] Considering these long spacings and calculated molecular lengths, we can suppose that the medium chain and long chain **1(*n*)** have a tilt in the K1 phase by 38−43°. The tilt angles are approximately 10° smaller than the actual tilt angle (50°) obtained from the single crystal of **1(11)**.[20]

Observation of Thermal Phase Behavior via Light Microscopy. The thermal phase behavior and appearance of **1(*n*)** was observed using a polarized light microscope equipped with a variable temperature hot stage. The microscopy revealed that the long-chain bolaamphiphiles **1(*n*)** ($n = 13$, 14, 16, 18, and 20) all form stable mesophases. In particular, **1(18)** and **1(20)** form an enantiotropic mesophase on heating and cooling, while **1(13)**, **1(14)**, and **1(16)** form a monotropic mesophase only on cooling from the isotropic melt.[22] A fanlike texture of **1(20)** (Figure 3) and the XRD pattern all support a smectic A (SmA) phase assignment for **1(*n*)** ($n = 13$, 14, 16, 18, and 20). Short- and medium chain showed no such liquid crystalline phases. The obtained melting- and clearing-point temperatures of **1(*n*)** (T_m and T_c, respectively) are plotted against the oligomethylene chain length in Figure 4. The T_m was determined only for the first heating cycle since decomposition occurred upon melting. The T_c is lower than the T_m in monotropic **1(*n*)** ($n = 13$, 14, and 16) since the T_c was only measured on second heating after the mesophase formation from the isotropic melt.

Conformational Study by FT-IR. The CH_2 antisymmetric $\nu_{as}(CH_2)$ and symmetric $\nu_s(CH_2)$ stretching vibration frequencies and the CH_2 scissoring deformation [$\delta(CH_2)$] band frequency of **1(*n*)** plotted against the chain length are shown in Figures 5 and 6, respectively.

(20) Masuda, M.; Shimizu, T. *Carbohydr. Res.* **1997**, *302*, 139−147.
(21) Hentrich, F.; Diele, S.; Tschierske, C. *Liq. Cryst.* **1994**, *17*, 827−839.
(22) We observed pure liquid crystal phase domains and decomposed brownish melting domain on rapid cooling (−30 K min^{-1}) from isotropic melts of **1(*n*)** ($n = 13$, 14, and 16). The decomposition of the liquid crystal phase domains was enough slow to measure the T_c on second heating.

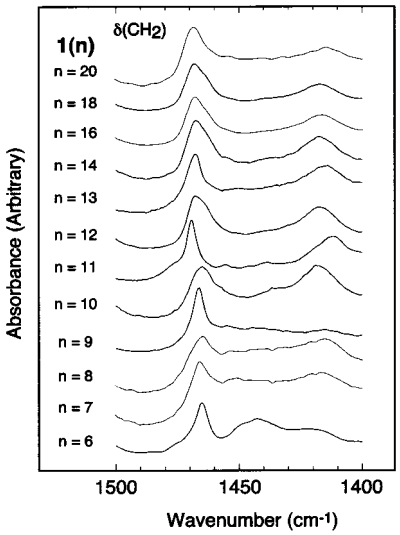

Figure 6. FT-IR spectra of the $\delta(CH_2)$ band region for the self-assembled **1(*n*)**.

Once again the dependence of the physical properties of the assemblies on the length of the alkylene spacer chain is readily apparent. The $\nu_{as}(CH_2)$ and $\nu_s(CH_2)$ stretching vibrations for alkylene chains generally absorb strongly around 2918−2928 cm^{-1} and 2850−2860 cm^{-1}, respectively. However, both the $\nu_{as}(CH_2)$ and $\nu_s(CH_2)$ band frequencies of the medium- and long chains are relatively low (2917−2920 and 2848−2851 cm^{-1}, respectively, corresponding to an all-*trans* conformation), while the short-chain homologues show a relatively high-frequency absorption (2923−2928 and 2852−2860 cm^{-1} respectively, corresponding to a *gauche*-including conformation).[23−25] The $\nu_{as}(CH_2)$ band frequency (2925.2 cm^{-1}) of **1(9)** is in conflict with all-*trans* chain conformation, but the $\nu_s(CH_2)$ band frequency and the nonpolymorphic nature support the classification of **1(9)** into the medium-chain category.

The $\delta(CH_2)$ band shown in Figure 6 directly reflects the oligomethylene chain packing and displays a pronounced even−odd effect on the $\delta(CH_2)$ band shape which provides strong evidence for an all-*trans* conformation in the medium- and longer chains ($\geq C_9$).[19] The $\delta(CH_2)$ bandwidth of the medium-chain bolaamphiphiles **1(*n*)** ($n \geq 11$, $n = 9$) shows an alternating feature with respect to the even−odd carbon numbers of the spacer chains (Figure 6). The even-numbered long-chain derivatives show the similar band shape as that of the medium chains. In contrast, the short-chain derivatives **1(*n*)** ($n \leq 8$, and $n = 10$) gave only broad bands and exhibited no clear even−odd alternating phenomena, which suggest the conformational difference between the short- and medium chain. The odd-numbered medium-chain derivatives **1(*n*)** ($n = 9$, 11, and 13) give sharp peaks with full width at half-maximum (fwhm) of 4−7 cm^{-1} representing a $T_{||}$ chain packing for **1(9)** and **1(11)** and a distorted hexagonal chain packing for **1(13)** (see, Supporting Information).[26,27] X-ray single-crystal analysis of **1(11)**[20] and XRD measurement are in good agreement with this packing mode.[19] In contrast, the even-numbered medium- and long-chain derivatives **1(*n*)** ($n = 12$, 14, 16, and 18) displayed a broad peak at 1467 cm^{-1} with fwhm of 9.5−10.6 cm^{-1} which can be ascribed to a slightly distorted $O_\perp$ chain packing or a mixture of $T_{||}$ and $O_\perp$ chain packing. This even−odd effect of the medium- and long chain on the FT-IR bands was further demonstrated by alternating *d* spacings observed in the small angle XRD measurements of **1(*n*)** ($n = 11$−14) (Figure 2).

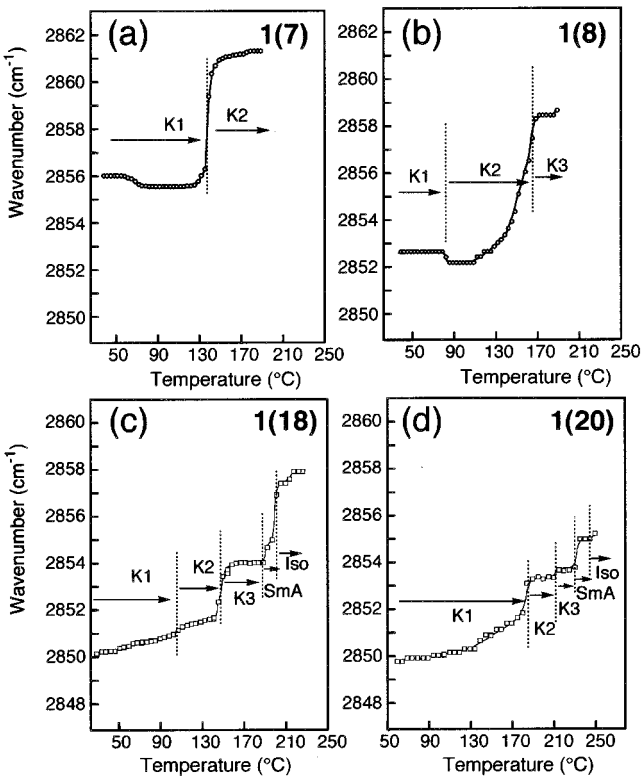

Figure 7. Temperature dependence of the $\nu_s(CH_2)$ band peak position for the self-assembled **1(*n*)** [(a) $n = 7$, (b) $n = 8$, (c) $n = 18$, and (d) $n = 20$] on first heating.

Variable Temperature FT-IR (VT-IR). Figures 7a−d show the temperature dependence of the $\nu_s(CH_2)$ band for representative short- ($n = 7$ and 8) and long-chain derivatives **1(*n*)** ($n = 18$ and 20) on the first heating cycle, with the $\nu_s(CH_2)$, amide I, and II bands of **1(*n*)** in each phase summarized in Table 2. The $\nu_s(CH_2)$ and amide I bands of the *gauche*-including short-chain derivatives **1(7)** and **1(8)** displayed a discontinuous shift to a higher frequency at the K1−K2 of **1(7)** or K2−K3 of **1(8)** phase transition, indicating the increase in *gauche* conformation and partial dissociation of amide hydrogen bonds. While the $\nu_s(CH_2)$ band of the short chain **1(8)** showed a small shift (0.5 cm^{-1}) to lower frequency at the K1−K2 transition (Figure 7b and Table 2), the band frequency in the K2 phase of **1(8)** still indicated a *gauche*-including conformation.

In contrast to the short-chain homologues, the all-*trans* long-chain derivatives **1(*n*)** transformed into other all-*trans* chain phases at the K1−K2 phase transition, and then *gauche*-including chain phase (K3). The oligomethylene chain of **1-(18)** in the K2 phase, which is a typical example of the long chain, still keeps an all-*trans* conformation since the frequency of the $\nu_s(CH_2)$ band is around 2851 cm^{-1} (Figure 7c). However, a higher frequency shift of this $\nu_s(CH_2)$ band to approximately 2854 cm^{-1} in the K3 phase suggested the transformation of the octadecane chain from an all-*trans* state into a *gauche*-including conformation. In addition, the wide-angle XRD patterns of K1, K2, and K3 phases indicated higher-order packing rather than

(23) Snyder, R. G.; Hsu, S. L.; Krimm, S. *Spectrochim. Acta, Part A* **1978**, *34*, 395−406.
(24) Snyder, R. G.; Strauss, H. L.; Elliger, C. A. *J. Phys. Chem.* **1982**, *86*, 5145−5150.
(25) Mantsch, H. H.; McElhaney, R. N. *Chem. Phys. Lipids* **1991**, *57*, 213−226.
(26) Snyder, R. G. *J. Mol. Spectrosc.* **1961**, *7*, 116−144.
(27) Garti, N.; Sato, K. *Crystallization and Polymorphism of Fats and Fatty Acids*; Marcel Dekker: 1988.

Table 2. VT-IR Absorption Bands of Self-Assembled Bolaamphiphiles **1(*n*)**

		VT-IR data (cm^{-1})		
chain length (*n*)	phase	$\nu_s(CH_2)$	amide I	amide II
6	K1	2860.5	1657	1559, 1540
	K2	n.d.[a]	1659	1550
7	K1	2856.7	1659	1577, 1559
	K2	2860.3	1667	1531
8	K1	2852.7	1662	1549
	K2	2852.0	1661	1530
	K3	2856	1669	1533
10	K1	2852.2	1662	1549
	K2	2848.3	1662	1528
	K3	2856.5	1673	1529
14	K1	2849.0	1661	1534
	K2	2850.1	1660	1530
	K3	2854.3	1669	1527
16	K1	2849.0	1658	1531
	K2	2851.2	1657	1527
	K3	2853.6	1671	1525
18	K1	2848.9	1658	1548
	K2	2851.7	1657	1545
	K3	2854.1	1670	1528
	SmA	2855.1	1676	1511
20	K1	2849.5	1636	1546
	K2	2853.2	1671	1529
	K3	2853.6	1671	1521
	SmA	2853.9	1673	1509

[a] Not determined.

a distorted hexagonal arrangement. The hydrogen bonds between amide groups are, however, partly dissociated.

The oligomethylene chains of **1(18)** and **1(20)** in the SmA phase melt at 236 °C and 228 °C, respectively with the $\nu_s(CH_2)$ band shifting to a higher frequency around 2855 cm^{-1} (Figure 7c and d) with partial dissociation of the amide hydrogen bonds occurring at the same time (Table 2).

Discussion

Phase Transition Behavior. Figure 8 shows a schematic illustration of the conformational and thermal phase behavior observed for **1(*n*)**. On heating from room temperature, the short chain-containing **1(*n*)** ($n = 6$, 7, 8, and 10) and the long-chain homologues **1(*n*)** ($n = 14$, 16, 18, and 20) exhibit a crystalline polymorphism, while the medium-chain derivatives **1(*n*)** ($n =$ 9, 11, 12, and 13) show no polymorphism. The short-chain derivatives **1(*n*)** in the self-assembled state include a *gauche* conformation with hydrogen-bonding headgroups at both ends. On heating, this *gauche*-including chain transformed into other highly *gauche*-including chains with weakly hydrogen-bonded headgroups. Finally the chain melts and takes random conformations. The K2 phase of the short chain **1(10)** deviates from this behavior. The decamethylene chain is in the intermediate range between the short- and medium chain, taking an all-*trans*-(K2) or *gauche*-including conformation (K1 and K3) and displaying both short- and medium-chain properties. In terms of polymorphism, **1(10)** should be categorized in the short chain rather than the medium one. As a result, the increase in *gauche*-conformation for the short-chain derivatives is in good agreement with the shrinkage of the long spacing *d* on heating (Figure 2). On the other hand, the spacer conformation of the long-chain homologues changed from an all-*trans* (K1 phase) into an all-*trans* (K2 phase, not shown in Figure 8) and finally into a *gauche*-including (K3 phase) or melting (SmA) phase. The widening of *d* for the long-chain derivatives arises from the decrease in a tilt angle within the layered structure with increasing thermal motion. Further, the *d* value became narrow in the smectic A phase.

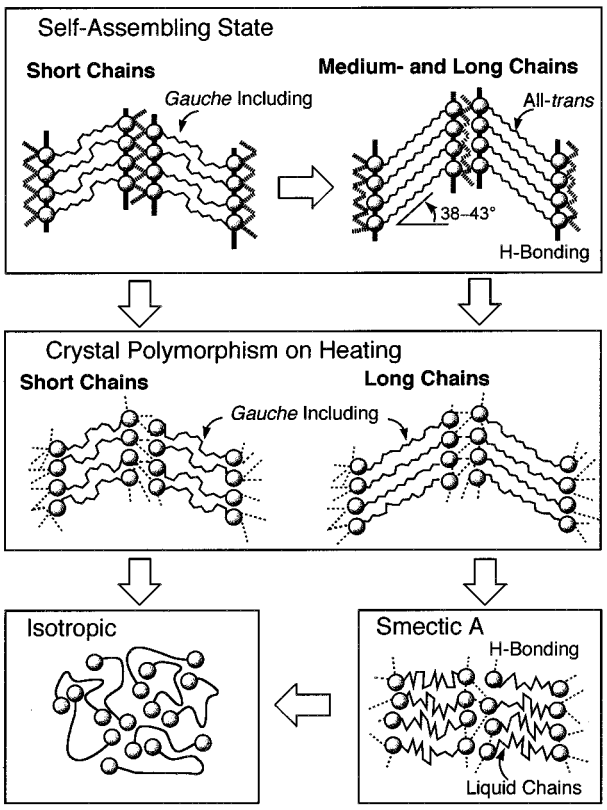

Figure 8. Schematic illustration of conformational changes in the self-assembled state of 1-glucosamide bolaamphiphiles **1(*n*)** and their thermal phases.

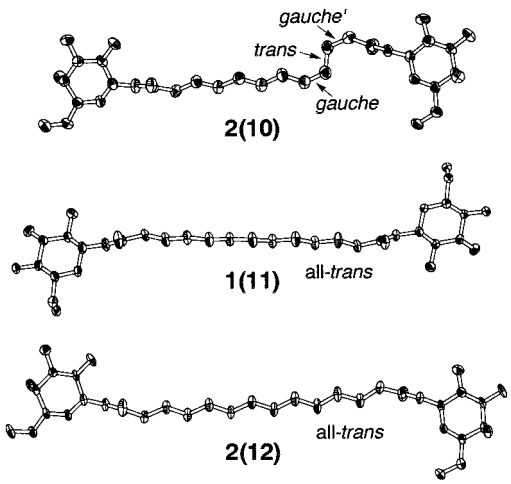

Figure 9. Crystal structures of **1(11)**, **2(10)**, and **2(12)**. Thermal ellipsoids are drawn at 50% probability.

The *gauche*-including structure, much higher phase transition temperatures, and complex polymorphism are characteristic of the 1-aldosamide bolaamphiphiles in contrast to one-head one-tail amphiphiles that often show only crystalline and mesogenic phases. The characteristic phase transition behavior is also strongly dependent on the oligomethylene spacer length.

Oligomethylene Chain Conformation in Self-Assembled Structures. The oligomethylene chain conformations of **2(10)**, **1(11)**, and **2(12)** derived from single-crystal X-ray analyses are shown in Figure 9. They are in good agreement with the structure inferred from an analysis of the $\nu_s(CH_2)$ band since **2**(**10**) adopts a *gauche*-including conformation and absorbs at a higher frequency than **1**(**11**) and **2**(**12**) (2852.7, 2848.9 and 2850.3 cm^{-1}, respectively). The $\nu_s(CH_2)$ band is well-known

as a useful probe for the detection of gel-to-liquid crystalline phase transition in lipids[25,28,29] with its advantage being that it appears separately from other vibration modes.[29] In general, the frequencies of the $\nu_{as}(CH_2)$ and $\nu_s(CH_2)$ bands shift from 2919 and 2850 cm^{-1} to 2923 and 2853 cm^{-1} respectively, as the *gauche/trans* conformer ratio in the alkyl chains increases upon the gel-to-liquid crystalline phase transition.[25,30,31] The frequencies of both bands and all of the FT-IR results support a change in the K1 phase oligomethylene chain conformation of **1(*n*)** from a *gauche*-including to an all-*trans* conformation as the chain length increases from $n = 10$ to $n = 12$ for even-numbered, and $n = 7$ to $n = 9$ for odd-numbered chains. A similar chain length effect was also observed for 2-glucosamide bolaamphiphiles **3(*n*)** ($n = 9-14$, 16, and 18).[32]

Molecular Dynamics Simulation. We have performed a molecular dynamics simulation for the **2(10)** and **1(11)** crystals to clarify the conformational change.[33] The following dynamics simulation results are in good agreement with the molecular structures in crystal. Thus, we found that a conformational change of the oligomethylene spacer from an all-*trans* to a *gauche*-including conformation when the dumbbell-shaped bolaamphiphiles with hydrogen-bonded headgroups self-assemble to form stable layered assemblies. The oligomethylene chain conformation of **2(10)** and **1(11)** in the crystal lattice could be modeled using a molecular dynamics simulation of the self-assembly.[33] An extended oligomethylene chain of **2(10)** generated as an initial structure[10] transformed dynamically into a *gauche*-including conformation within 100 ps at 100 K and 0.1 MPa. However, the extended conformation of **1(11)** extracted from crystal analysis[20] persisted under the same conditions. Interestingly the *kink* conformation of **2(10)** generated by the molecular simulation appeared at the same position as that found in the X-ray crystal structure,[10] suggesting that the oligomethylene moieties around the amide linkage are likely to be strained.

Energetics. To clarify the intermolecular interactions involved, we calculated the intermolecular potential energy for dimers of **2(10)** and **1(11)** with displacement of the relative arrangement of the mass center from the equilibrium position along *a*, *b*, and *c* axes. The energetics indicated a strong intermolecular interaction between the sugar headgroups.[33] The intermolecular interaction for **2**(**10**) and **1**(**11**) could be broken down into hydrogen-bonding (HB, -5.7 and -10.4 kJ mol^{-1} for **2(10)** and **1(11)**, respectively), electrostatic (ES, -10.4 and -16.9 kJ mol^{-1}), and van der Waals (vdW, -11.6 and -10.6 kJ mol^{-1}) components.[34] The total energy of ES and HB, which derive mainly from interactions between the polar headgroups, are bigger than the van der Waals interaction in each bolaamphiphile. The HB and ES energies are also much bigger than those found for common phospholipids.[35] In the crystal lattice of **2(10)** and **1(11)**, we have found 26 and 24 hydrogen bonds, respectively. This means that the two headgroups are linked rigidly together via multiple hydrogen bonds leading to a network that behaves as a semirigid framework.

The conformational disorder of the short-chain spacer from the all-*trans* conformation mentioned in the above VT-XRD and FT-IR section arises from three causes: (1) the flexibility of the oligomethylene chain compared with the rigidity of the hydrogen-bonded networks, (2) the difference in the limiting molecular area between the pyranosamide ring (0.4 nm^2/molecule)[36] and the oligomethylene chain (0.2 nm^2/molecule),[27] and (3) the impossibility of the oligomethylene chains adopting an interdigitated packing in the MLM structures. The dominant packing interaction of the bulky headgroup thus imposes constraints on the flexible chains. As a result, the packing of the sugar moiety has a significant influence on the conformation of the short chain ($n \leq 8$, and $n = 10$) and eventually introduces a *kink* conformation in the bolaamphiphiles. On the other hand, the packing energy of the all-*trans* conformer can be considered to be predominant for the long-chain bolaamphiphiles ($n \geq 14$) since the chain elongation stabilizes the hydrophobic interaction. As a result, the all-*trans* conformation was kept even in the K2 phase. The molecular area difference between the headgroup and the oligomethylene chain can be compensated for by tilt and shrinkage of the flexible oligomethylene chains.[10,20] The headgroup packing interaction will be balanced in the nonpolymorphic medium-chain derivatives ($n = 9$, 11, 12, and 13) by the chain packing interaction with the all-*tarns* conformation. Further, the unbalanced headgroup and chain-packing interactions would induce the polymorphism for the short and medium-chain bolaamphiphiles.

Stereochemical Effect on Mesogenic Properties. The smectic phase described previously represents the first example of a liquid crystalline phase for aldosamide bolaamphiphiles. Only long chain **1(*n*)** showed stable mesophase since the mesophase of the medium chain **1(13)** was unstable. The T_m and T_c of **1(*n*)** showed relatively high temperatures when compared with those of other, structurally similar bolaamphiphilic tetraols[21] or gemini-type sugar-based amphiphiles.[37,38] These one-head one-tail 1-aldosamides,[39,40] also show higher melting- and clearing points than *n*-alkyl β-glucopyranosides. The increased thermal stability of **1(*n*)** stems from hydrogen-bond formation between amide groups as well as strong intermolecular interactions from double headgroups since the amide hydrogen bond chain enhances the molecular ordering and enforces the formation of hydrogen bonding between the sugar hydroxyl groups. The VT-IR spectra also indicate that the hydrogen bonds between the amide groups remain as a dynamic linkage even in the SmA phase. The change in the substituted position of the oligomethylene spacers also affects the liquid crystallinity. The 2-glucosamide bolaamphiphiles **3(*n*)** ($n = 9-14$, 16, and 18)[32] formed no liquid crystalline phase merely decomposing at the melting point. The lack of mesogenicity of **3(*n*)** derives from the formation of strong hydrogen bonds between the 2-glucosamide moieties, also resulting in a drastic reduction in the solubility of **3(*n*)** in a variety of solvents.[32]

Two possible molecular models can be drawn for the molecular arrangement in this mesophase. One is a monolayered

(28) Wallach, D. F. H.; Verma, S. P.; Fookson, J. *Biochim. Biophys. Acta* **1979**, *559*, 153−208.
(29) Casal, H. L.; Mantsch, H. H. *Biochim. Biophys. Acta* **1984**, *779*, 381−401.
(30) Snyder, R. G.; Schaachtschneider, J. H. *Spectrochim. Acta* **1963**, *19*, 85−116.
(31) Parikh, A. N.; Schivley, M. A.; Koo, E.; Seshadri, K.; Aurentz, D.; Mueller, K.; Allara, D. L. *J. Am. Chem. Soc.* **1997**, *119*, 3135−3143.
(32) Nakazawa, I.; Masuda, M.; Okada, Y.; Hanada, T.; Yase, K.; Asai, M.; Shimizu, T. *Langmuir* **1999**, *19*, 4757−4764.
(33) Mikami, M.; Matsuzaki, T.; Masuda, M.; Shimizu, T.; Tanabe, K. *Comput. Mater. Sci.* **1999**, *14*, 267−276.
(34) The intermolecular potential energy was calculated along with the *a* axis which was the dominant intralayer interaction in the crystal lattice.
(35) Stouch, T. R.; Ward, K. B.; Altieri, A.; Hagler, A. T. *J. Comput. Chem.* **1991**, *12*, 1033−1046.
(36) Abe, Y.; Harata, K. *Langmuir* **1996**, *12*, 636−640.
(37) Auzely-Velty, R.; Benvegnu, T.; Plusquellec, D.; Mackenzie, G.; Haley, J. A.; Goodby, J. W. *Angew. Chem., Int. Ed.* **1998**, *37*, 2511−2515..
(38) Pestman, J. M.; Terpstra, K. R.; Stuart, M. C. A.; Doren, H. A. v.; Brisson, A.; Kellogg, R. M.; Engberts, J. B. F. N. *Langmuir* **1997**, *13*, 6857−6860.
(39) Ewing, D. F.; Goodby, J. W.; Haley, J. A.; Kelly, S. M.; Lettelier, P.; Mackenzie, G. *Liq. Cryst.* **1997**, *23*, 759−769.
(40) Ewing, D. F.; Glew, M.; Goodby, J. W.; Haley, J. A.; Kelly, S. M.; Komanschek, B. U.; Letellier, P.; Mckenzie, G.; Mehl, G. H. *J. Mater. Chem.* **1998**, *8*, 871−880.

Scheme 2

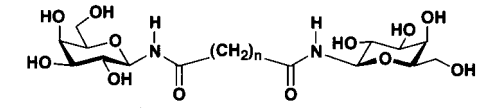

2(n): n = 10, 11, and 12

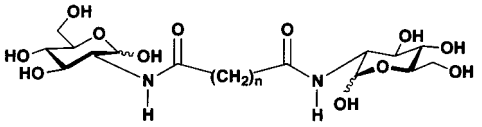

3(n): n = 9–14, 16, and 18

aggregate, and the other is a bilayered aggregate with U-shaped molecules. The monolayered structures are observed in the single crystals of **1(11)**, **2(10)**, and **2(12)**, strongly supporting the former as a self-assembly motif.

Relation of Fiber Formation and Chain Length. The aldosamide bolaamphiphiles **1(*n*)**, **2(*n*)**, and **3(*n*)** form intermolecular multiple hydrogen bonds between the sugar hydroxyls and between the amide groups which are not well solvated by hydrophilic solvents and do not form a lyotropic mesophase. In addition, while **1(*n*)** ($n = 10$, 12, 14, and 16) and **3(*n*)** ($n = 10$, 12, 14) form helically twisted fibers in water, no chiral smectic phases could be observed. Even−odd effects on the morphology[19] of fibers formed for **1(*n*)** appear only for the extended chain conformations observed in medium- and long chain **1(*n*)**. This is because the strongly interacting groups such as amide and sugar hydroxyl groups are linked to the ends of the oligomethylene chains, and thus the relative arrangements of the two headgroups in **1(*n*)** change, depending on the even−odd carbon numbers in the extended chain (see Schemes 1 and 2).

Conclusions

On the basis of the conformational properties of their oligomethylene chains, a family of 1-glucosamide bolaamphiphiles **1(*n*)** have been categorized into three groups: short- ($6 \leq n \leq 8$, and $n = 10$), medium- ($n = 9$, and $11 \leq n \leq 13$), and long chain ($14 \leq n \leq 20$). Short chains **1(*n*)** display a *gauche*-including conformation, whereas medium- and long chains **1(*n*)** adopt an all-*trans* conformation. On heating, the short- and long-chain bolaamphiphiles produced a crystal polymorphism with the short chain **1(*n*)** giving *gauche*-including phases and the long-chain homologues an all-*trans* chain phase (K1 and K2), a *gauche*-including chain phase (K3), and melting chain phase (smectic A).

Experimental Section

Materials. All 1-glucosamide bolaamphiphiles **1(*n*)** were synthesized in a fashion similar to those previously described elsewhere.[41] The chemical and physical data for new compounds **1(16)** and **1(20)** are described here.

1(16): platelet crystals; ^{1}H NMR (600 MHz, DMSO-d_6 and D_2O one drop, 60 °C) δ 4.71 (d, $J = 8.9$ Hz, 2H, H-1), 3.64 (dd, $J = 11.9$ and 2.0 Hz, 2H, H-6b), 3.43 (dd, $J = 11.9$ and 5.0 Hz, 2H, H-6a), 3.21 (dd, $J = 8.6$ and 8.2 Hz, 2H, H-3), 3.14 (m, $J = 8.9$, 5.0, and 2.0 Hz, 2 Hz, 2H, H-5), 3.10 (dd, $J = 8.9$ and 8.2 Hz, 2H, H-4), 3.08 (dd, $J = 8.9$ and 8.6 Hz, 2H, H-2), 2.10 (t, $J = 7.6$ and 7.3 Hz, 4H, $-CH_2-$CONH−), 1.50 (m, 4H, $-CH_2-CH_2-$CONH), 1.25 (m, 24H, $-CH_2-$). Anal. Calcd for $C_{30}H_{56}N_2O_{12}$: C, 56.59; H, 8.86; N, 4.40. Found: C, 56.57; H, 8.87; N, 4.56.

1(20): platelet crystals; ^{1}H NMR (DMSO-d_6 and D_2O one drop, 60 °C) δ 1.25 (m, 32H, $-CH_2-$); otherwise similar data as for **1(16)**. Anal. Calcd for $C_{34}H_{64}N_2O_{12}$: C, 58.94; H, 9.31; N, 4.04. Found: C, 58.90; H, 9.28; N, 4.14.

Preparation of the self-assemblies from an aqueous solution has been reported elsewhere.[19]

Temperature Control. During the VT-IR, VT-XRD, melting-, and clearing-point measurements on polarized microscopy analyses, temperatures were controlled using a Mettler FP82 hot stage linked to a Mettler FP90 with an accuracy of ±0.4 °C. The heating rate for all variable temperature measurements was 5 K min^{-1}.

DSC. Weighed, anhydrous samples were placed into an aluminum pan, and the pan was sealed. Heating and cooling scans over the temperature range 20−300 °C were performed on a Seiko DSC 6100 differential scanning calorimeter equipped with a nitrogen gas cooling unit.

FT-IR. Infrared spectra were measured using a (JASCO FT-620 and Micro-20/FT/IR-620) Fourier transform spectrometer operating at 2 cm^{-1} resolution with an unpolarized beam striking the sample at normal incidence. All spectra were reported in absorbance *A*: Negative logarithm to the base 10 of the transmittance *T*, $A = -\log(T)$, where *T* is ratio of the radiant power transmitted by the sample (*I*) to the radiant power incident on the sample (I_0), $T = I/I_0$.

Preparation for FT-IR samples. Grounded samples of crystalline powder (0.2 mg) were sandwiched between KBr crystal plates (7 × 7 × 1 mm), and then pressed to suppress the scattering to the incident radiation. The transparent disks obtained (10 mm in diameter and 1.5 mm in thickness) were used for the FT-IR and VT-IR measurements.

XRD. X-ray diffraction patterns were measured using a Rigaku diffractometer (Type 4037) using graded *d*-space elliptical side-by-side multilayer optics, monochromated Cu Kα radiation (40 kV, 30 mA), and imaging plate (R-Axis IV). The typical exposure time was 10 min for solid phases and 5 min for liquid crystalline phases with 150-mm camera length.

Thermal Optical Light Microscopy. The melting- and clearing points were measured on the first heating cycle using a polarized light microscope (Olympus BX50), and optical images were recorded with 3-CCD video camera (Olympus CS520MD).

Acknowledgment. We thank Dr. M. Goto for the discussion of the X-ray diffraction data. We thank also Dr. A. Murphy and Mr. I. Nakazawa for the valuable discussions. This work was supported by New Energy and Industrial Technology Development Organization (NEDO) for the project on Technology for Novel High-Functional Materials Program, AIST, MITI.

Supporting Information Available: Tables of IR $\nu_{as}(CH_2)$ and $\nu_s(CH_2)$ band features and temperature dependence, band frequencies for all compounds, thermal parameters of DSC, and all of the XRD diagrams (PDF). This material is available free of charge via the Internet at http://pub.acs.org.

JA001884P

(41) Masuda, M.; Shimizu, T. *J. Carbohydr. Chem.* **1998**, *17*, 405−416.